Wind Energy Conversion System using DFIG Controlled by Backstepping and Sliding Mode Strategies

Nihel Khemiri*, Adel Khedher**, Mohamed Faouzi Mimouni***

*Research unit ESIER, National Engineering School of Monastir ENIM, Tunisia

**Research unit RELEV, National Engineering School of Sfax ENIS, National Engineering School of Sousse ENISo, Tunisia

***National Engineering School Monastir ENIM, Tunisia

‡Corresponding Author; Nihel Khemiri, City Elbaloui 1 Street Haffouz 3100 Kairouan, Tunisia,
+216 92 129 693,khemirin@yahoo.fr

Received: 20.05.2012 Accepted:05.08.2012

Abstract- In this paper we present the modeling and control designs for a variable-speed constant-frequency wind energy conversion system using double fed induction generator (DFIG). The aim of this paper is to design and compare two distinct control strategies to control the rotor side converter and two control strategies to control the grid side converter. For the rotor side converter (RSC), a backstepping control strategy is firstly developed. Secondly, a sliding mode control strategy is presented. The same strategies to control the grid side converter (GSC). Simulation results using Matlab/Simulink have shown good performances of the wind energy converter system operate under typical wind variations and every propose control strategies.

Keywords- DFIG, Backstepping, Sliding Mode Control, Rotor Side Converter, Grid Side Converter

1. Introduction

The mainstream high-power wind-energy conversion systems (WECSs) are based on doubly-fed induction generators (DFIGs). The stator windings of DFIGs are directly connected to the grids, and rotor windings are connected to the grids through back-to-back power electronic converters. The back-to-back converter consists of two converters, i.e., rotor side converter (RSC) and grid side converter (GSC) that are connected "back-to-back." Between the two converters a dc-link capacitor is placed, as energy storage, in order to keep the voltage variations in the dc-link voltage small. Control of the DFIG is more complicated than the control of a standard induction machine. In order to control the DFIG the rotor current is controlled by a power electronic converter. Various control strategies have been developed in the literature [1,2,3,4].

The classical control strategies for DFIG are normally based on voltage oriented control (VOC) algorithms [5]. In the past few decades it suffers from the problem of the machine parameters variations, which comes to compromise the robustness of the control device.

Therefore, the controller should accommodate the effects of uncertainties and keep the system stable against a large variation of system parameters. The conventional PI-based controllers cannot fully satisfy stability and performance requirements. On the other hand, the system is highly nonlinear and has a large range of operating points. Thus, linearization around one operating point cannot be employed to design the controller. Nonlinear control methods can be used to effectively solve this problem [6] and [7].

In attempt to achieve high performances in the steady state as well as during the transients, a different nonlinear control structure must be applied. In the recent two decades, many modified nonlinear state feedback such as input-output feedback linearization control and sliding mode have been applied to more improve the control performances [8].

The aim of this paper is to present, discuss and compare various control strategies for DFIG driven by wind turbine

under typical wind variations. For the both RSC and GSC, a backstepping control (BS) strategy is firstly developed. Secondly, a sliding mode control (SMC) strategy is presented.

The backstepping theory is a systematic and recursive design methodology for non linear feedback control, the derived algorithm backstepping, replacing the PI controller into FOC structure, can give improved tracking response. With these control algorithms, the feedback control laws are easily constructed and associated to *Lyapunov* functions. The sliding mode control is nowadays frequently used because of its simplicity and efficiency, it is not sensible to parameters variations and externals disturbances. The use of this control mode can be justified by the required high performances required and robustness of the WECS operation.

This paper is organized as follows: in the second section, we present the modeling of the wind energy system. We modeled the DFIG in the first step and the wind turbine in the second step. Third section presents the control strategies of the RSC. Firstly, we propose a backsteppping control. Then, the SMC principle is developed. Fourth section, studies the control of electrical system in the GSC. Firstly, we propose a backsteppping control. Then, the SMC principle is developed. Simulation results are presented and discussed in the fifth section and we finish by a conclusion.

Dynamic modeling and simulation of the DFIG-wind turbine power generation system, backstepping and sliding mode controllers are performed by means of Matlab/Simulink.

2. Modelling of the Wind Generation System

2.1. Modeling of the DFIG

In complex notation, the DFIG equations are derived from *Park* model expressed in a reference frame d-q rotating at synchronous speed ω_s. The electrical energy conversion system is described by the equations of induction machines given by [9]:

$$\begin{cases} \overline{V}_s = R_s\bar{i}_s + \frac{d\overline{\varphi}_s}{dt} + j\omega_s\overline{\varphi}_s \\ \overline{V}_r = R_r\bar{i}_r + \frac{d\overline{\varphi}_r}{dt} + j\omega_r\overline{\varphi}_r \end{cases} \quad (1)$$

With:

i being the current (A), V is the voltage (V), R_s and R_r are respectively stator and rotor resistance (Ω), ω_s angular speed of the rotating field referred to the stator (rad/s), ω_r angular speed of the rotating field referred to the rotor (rad/s). $\overline{\varphi}_s$ and $\overline{\varphi}_r$ are respectively stator and rotor flux (Wb). Where:

$$\begin{cases} \overline{\varphi}_s = L_s\bar{i}_s + M\bar{i}_r \\ \overline{\varphi}_r = L_r\bar{i}_r + M\bar{i}_s \end{cases} \quad (2)$$

Using complex stator and rotor space vector currents, the electromagnetic torque generated by the DFIG is given by:

$$T_{em} = \frac{3}{2}\frac{n_p M}{L_s}\,\Im\mathrm{m}(\bar{i}_r\bar{i}_s^*) \quad (3)$$

The active and reactive powers exchanged between the stator and the grid can be expressed as follows:

$$\begin{cases} P_s = \frac{3}{2}\Re e\left(\overline{V}_s\bar{i}_s^*\right) \\ Q_s = \frac{3}{2}\Im\mathrm{m}(\overline{V}_s\bar{i}_s^*) \end{cases} \begin{cases} P_s = \frac{3}{2}\Re e\left(\overline{V}_s\bar{i}_s^*\right) \\ Q_s = \frac{3}{2}\Im\mathrm{m}(\overline{V}_s\bar{i}_s^*) \end{cases} \quad (4)$$

The stator power P_s must check in permanent mode and the active power injected with the node of generator and grid connection is given by:

$$\begin{cases} P_s = P_{aeor} + P_r \\ P_g = P_s + P_o \end{cases} \quad (5)$$

P_{aeor} and P_r respectively, the wind available and the rotor powers.

Where:

$$\begin{cases} P_{aeor} = T_t\Omega_{meca} \\ P_r = T_t\omega_r \end{cases} \quad (6)$$

The power P_r depends directly on angular slip ω_r. That is to say extracted from the grid in sub-synchronous generating mode (ω_r>0) or is output in the grid in the case of an operation super-synchronous generating mode (ω_r<0) [10].

2.2. Modeling of the Wind Turbine

The mechanical energy conversion process is described by the equation of induction machines given by:

$$J\frac{d\omega}{dt} + f\omega = T_t - T_{em} \quad (7)$$

With

J: total moment of inertia.

The developed wind turbine torque can be written as:

$$T_t = \frac{\rho\pi R^2 V_v^3}{2\Omega_t}C_p \quad (8)$$

In this study, for each wind speed the rotational speed is varied to track the maximum power curve. The maximum mechanical power extracted from the wind turbine is expressed by:

$$P_t = \frac{\rho\pi R^2 V_v^3}{2}C_{p\,max} \quad (9)$$

2.3. General control structure

The studied system is composed by three-bladed rotor with a corresponding mechanical gearbox, a DFIG, two power converters (RSC and GSC), a DC-link capacitor, and a grid filter.

The GSC works as a rectifier and RSC works as an inverter. When the machine is driven above synchronous speed, power is recovered from the rotor with RSC working as a rectifier GSC working as an inverter. Control scheme include reactive and active power control is given by figure 1.

3. RSC Control

In this part, we present two control strategies. The first is a backstepping control. The second is the sliding mode control strategy.

3.1. Backstepping Control

The Backstepping control approach for the mechanical speed regulation and the flux generation can be better applied to replace the traditional non linear feedback proportional-integral PI control of the field oriented control technique for better performances.

3.1.1.Description model

The above model can be presented as differential equations for the rotor currents, the stator flux vector components under the following form:

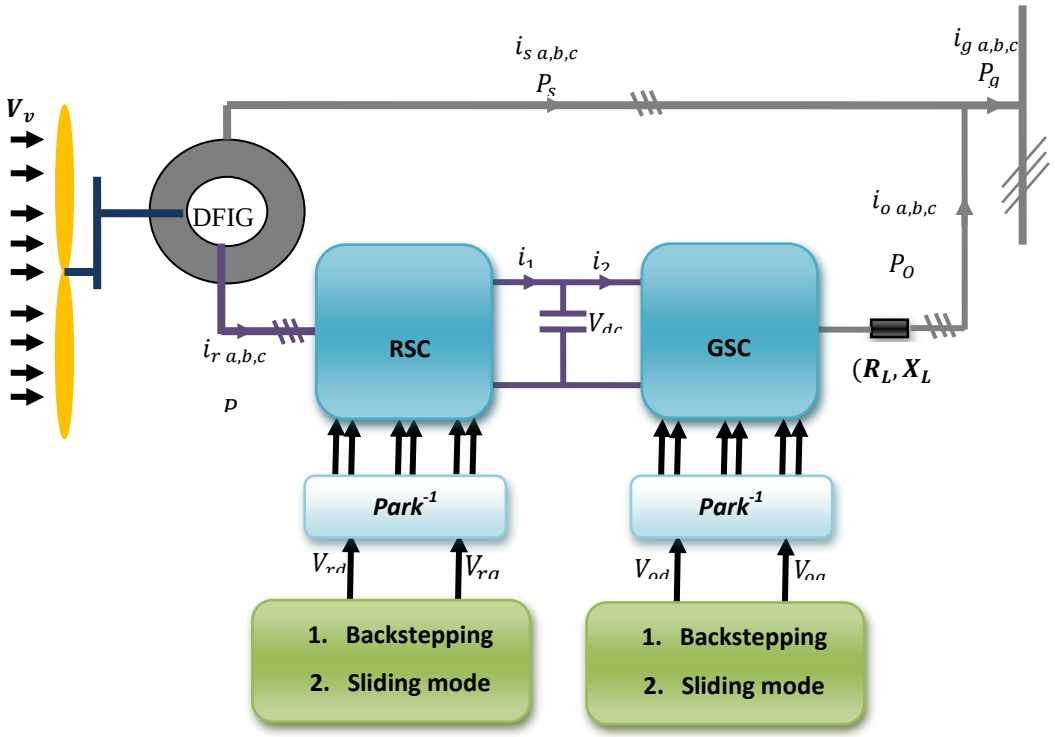

Fig. 1. Control Structure of the proposed WECS.

$$\begin{cases} \frac{di_{rd}}{dt} = \frac{1}{\sigma L_r}V_{rd} - \delta i_{rd} + \alpha R_s \Phi_{sd} + \beta V_{sd} + \omega_r i_{rq} \\ \frac{di_{rq}}{dt} = \frac{1}{\sigma L_r}V_{rq} - \gamma i_{rq} - \beta \omega_r \Phi_{sd} - \omega_r i_{rd} \\ \frac{d\Phi_{sd}}{dt} = -V_{sd} - \frac{R_s}{L_s}\Phi_{sd} + \frac{R_s M}{L_s} i_{rd} \\ \frac{d\Omega}{dt} = \frac{T_t}{J} - \frac{f}{J}\Omega - \frac{T_{em}}{J} \end{cases} \quad (10)$$

The electromagnetic torque is given by the following expression:

$$T_{em} = -\mu \Phi_{sd} i_{rq} \quad (11)$$

Where the state variables are the rotor currents (i_{rd}, i_{rq}), the stator flux (Φ_{sd}) and the mechanical speed Ω. The rotor voltages (V_{rd}, V_{rq}) are considered as the control variables, with:

$$\delta = \frac{R_r L_s^2 + M^2 R_s}{\sigma L_r L_s^2}, \qquad \alpha = \frac{M}{\sigma L_r L_s^2}, \qquad \beta = \frac{M}{\sigma L_r L_s},$$

$$\gamma = \frac{R_r}{\sigma L_r}, \qquad \mu = \frac{3}{2} p \frac{M}{L_s}$$

Accounting for eq. (11), the DFIG equations given by eq. (10) turn to be:

$$\begin{cases} \frac{d\Omega}{dt} = b_1 = \frac{T_t}{J} - \frac{f}{J}\Omega + \frac{\mu}{J}\Phi_{sd} i_{rq} \\ \frac{d\Phi_{sd}}{dt} = b_2 = -V_{sd} - \frac{R_s}{L_s}\Phi_{sd} + \frac{R_s M}{L_s} i_{rd} \\ \frac{di_{rd}}{dt} = b_3 + \frac{1}{\sigma L_r}V_{rd} = -\delta i_{rd} + \alpha R_s \Phi_{sd} + \beta V_{sd} + \omega_r i_{rq} + \frac{1}{\sigma L_r}V_{rd} \\ \frac{di_{rq}}{dt} = b_4 + \frac{1}{\sigma L_r}V_{rq} = -\gamma i_{rq} - \beta \omega_r \Phi_{sd} - \omega_r i_{rd} + \frac{1}{\sigma L_r}V_{rq} \end{cases} \quad (12)$$

The DFIG system, given by eq. (12), will be approximately decomposed in two decoupled subsystems. Hence, they are considered (Ω, i_{rq}) as state variables and V_{rq} as input command for the first subsystem, while (Φ_{sd}, i_{rd}) as state variables and V_{rd} as input command for the second one. The subsystem structure will be fully exploited in the backstepping control design as detailed in the next.

3.1.2. Control Design

The basic idea of the Backstepping design is the use of the so-called "virtual control" to systematically decompose a complex nonlinear control design problem into simpler,

smaller ones. Roughly speaking, Backstepping design is divided into various design steps [11]. In each step we essentially deal with an easier, single-input-single-output design problem, and each step provides a reference for the next design step. The overall stability and performance are achieved by a Lyapunov function for the whole system [12]. The synthesis of this control can be achieved in two steps.

(i) Step 1: Computation of the reference rotor currents

In the first step, it is necessary that the system follows given trajectory for each output variable [13]. To do so, a function $y_c = (\Omega_c, \Phi_c)$ is defined, where Ω_c and the Φ_c are the mechanical speed and stator flux references, respectively. The mechanical speed and stator flux tracking error e_1 and e_3 are defined by:

$$\begin{cases} e_1 = \Omega_c - \Omega \\ e_3 = \Phi_c - \Phi_{sd} \end{cases} \tag{13}$$

The derivative of Eq. (13) gives

$$\begin{cases} \dot{e}_1 = \dot{\Omega}_c - \dot{\Omega} \\ \dot{e}_3 = \dot{\Phi}_c - \dot{\Phi}_{sd} \end{cases} \tag{14}$$

Accounting for eq. (12), one can rewrite eq. (14) as follows:

$$\begin{cases} \dot{e}_1 = \dot{\Omega}_c - b_1 \\ \dot{e}_3 = \dot{\Phi}_c - b_2 \end{cases} \tag{15}$$

In order to check, let us the tracking performances choose the first *Lyapunov* candidate function V_1 associated to the stator flux and mechanical speed errors, such us [14]:

$$V_1 = \frac{1}{2}e_1^2 + \frac{1}{2}e_3^2 \tag{16}$$

Using eq. (15), the derivative of eq. (16) is written as follows:

$$\dot{V}_1 = e_1(\dot{\Omega}_c - b_1) + e_3(\dot{\Phi}_c - b_2) \tag{17}$$

This can be rewritten as follows:

$$\dot{V}_1 = -K_1 e_1^2 - K_3 e_3^2 \tag{18}$$

Where K_1, K_3 should be positive parameters [13], in order to guarantee a stable tracking, which gives:

$$\begin{cases} \dot{e}_1 = \dot{\Omega}_c - \dot{\Omega} = -K_1 e_1 \\ \dot{e}_3 = \dot{\Phi}_c - \dot{\Phi}_{sd} = -K_3 e_3 \end{cases} \tag{19}$$

Eq. (17) allows the synthesis of rotor current references, such as:

$$\begin{cases} (\Phi_{sd} i_{rq})_c = \frac{J}{\mu}\left(\dot{\Omega}_c - \frac{T_t}{J} + \frac{f}{J}\Omega + K_1 e_1\right) \\ (R_s i_{rd})_c = \frac{L_s}{M}\left(\dot{\Phi}_c + \frac{R_s}{L_s}\Phi_{sd} + K_3 e_3\right) \end{cases} \tag{20}$$

(ii) Step 2: Computation of the reference rotor voltages

In this step, an approach to achieve the current reference generated by the first step is proposed. Let us recall the current errors, such as:

$$\begin{cases} e_2 = (\Phi_{sd} i_{rq})_c - \Phi_{sd} i_{rq} \\ e_4 = (R_s i_{rd})_c - R_s i_{rd} \end{cases} \tag{21}$$

Accounting for eq. (20), eq. (21) turns to be:

$$\begin{cases} e_2 = \frac{J}{\mu}\left(\dot{\Omega}_{ref} - \frac{T_t}{J} + \frac{f}{J}\Omega + K_1 e_1\right) - \Phi_{sd} i_{rq} \\ e_4 = \frac{L_s}{M}\left(\dot{\Phi}_{sd-ref} + \frac{R_s}{L_s}\Phi_{sd} + K_3 e_3\right) - R_s i_{rd} \end{cases} \tag{22}$$

The derivative of eq. (21) yields:

$$\begin{cases} \dot{e}_2 = (\dot{\Phi}_{sd} i_{rq})_c - (\dot{\Phi}_{sd} i_{rq}) = A_1 - \frac{1}{\sigma L_r}\Phi_{sd} V_{rq} \\ \dot{e}_4 = (R_s \dot{i}_{rd})_c - (R_s \dot{i}_{rd}) = A_2 - \frac{R_s}{\sigma L_r} V_{rd} \end{cases} \tag{23}$$

Where A_1, A_2 are known signals that can be used in the control, and their expressions are as follows:

$$\begin{aligned} A_1 = f_a \ddot{\Omega}_{ref} - K_1^2 f_b e_1 + K_1 e_2 + f_c C_t - f_d \Omega \\ + (f_e + f_f + f_h)\Phi_{sd} i_{rq} - f_g i_{rd} i_{rq} \\ + \omega_r \Phi_{sd} i_{rd} + f_i \omega_r \Phi_{sd}^2 \end{aligned}$$

$$\begin{aligned} A_2 = f_j K_3^2 e_3 + K_3 e_4 + f_j \ddot{\Phi}_{sd-ref} - f_l \Phi_{sd} \\ + f_k i_{rd} - R_s \omega_r i_{rq} \end{aligned}$$

With

$$f_a = f_b = \frac{JL_s}{3M}, \quad f_c = \frac{fL_s}{3MJ}, \quad f_d = \frac{f^2 L_s}{3JM},$$

$$f_e = \frac{f}{J}, \quad f_f = \frac{R_s}{L_s}, \quad f_g = \frac{R_s M}{L_s},$$

$$f_h = \frac{R_r}{\sigma L_r}, \quad f_i = \frac{M}{\sigma L_s L_r}, \quad f_j = \frac{L_s}{M},$$

$$f_k = \frac{R_s^2}{L_s} + \frac{R_s R_r L_s^2 + M^2 R_s^2}{\sigma L_r L_s^2}, \quad f_l = \frac{R_s^2}{ML_s} + \frac{MR_s^2}{\sigma L_r L_s^2}, \; f_m = \frac{R_s}{M}$$

One can notice that eq. (23) include the system inputs: the rotor voltage. These could be find out through the definition of a new *Lyapunov* function based on the errors of the speed, of the stator flux and the rotor currents [15], giving by eq. (24):

$$V_2 = \frac{1}{2}(e_1^2 + e_2^2 + e_3^2 + e_4^2) \tag{24}$$

The derivative of eq. (24) is given by:

$$\dot{V}_2 = e_1\dot{e}_1 + e_2\dot{e}_2 + e_3\dot{e}_3 + e_4\dot{e}_4 \tag{25}$$

By setting eq. (20) in eq. (24), one can obtain:

$$\begin{aligned} \dot{V}_2 = -K_1 e_1^2 - K_2 e_2^2 - K_3 e_3^2 - K_4 e_4^2 \\ + e_2\left(\frac{\mu}{J}e_1 + A_1 - \frac{1}{\sigma L_r}\Phi_{sd} V_{rq} + K_2 e_2\right) \\ + e_4\left(\frac{M}{L_s}e_3 + A_2 - \frac{R_s}{\sigma L_r} V_{rd} + K_4 e_4\right) \end{aligned} \tag{26}$$

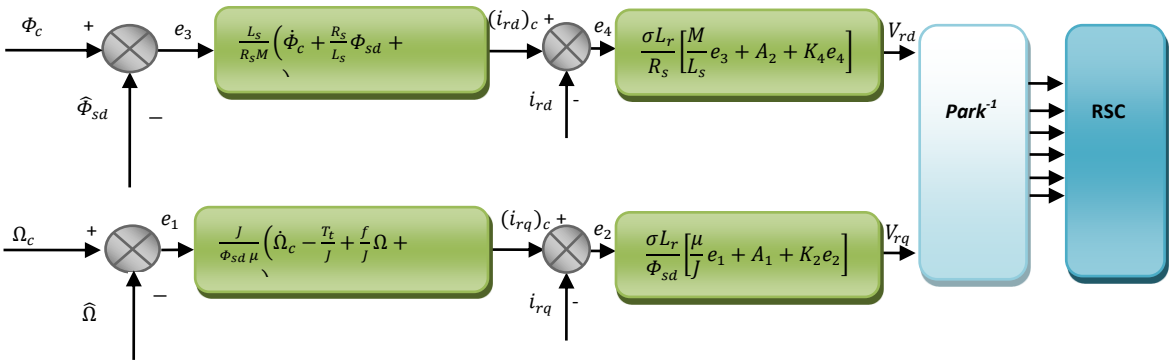

Fig. 2. Block Diagram of the proposed backstepping applied to the RSC of WECS based on DFIG.

The derivative of the complete *Lyapunov* function eq. (26) can be negative definite, if the quantities between parentheses in eq. (26), would be chosen equal to zero.

$$\begin{cases} \frac{\mu}{J}e_1 + A_1 - \frac{1}{\sigma L_r}\Phi_{sd}V_{rq} + K_2 e_2 = 0 \\ \frac{M}{L_s}e_3 + A_2 - \frac{R_s}{\sigma L_r}V_{rd} + K_4 e_4 = 0 \end{cases} \quad (27)$$

The rotor voltages then deduced as follows:

$$\begin{cases} V_{rd} = \frac{\sigma L_r}{R_s}\left[\frac{M}{L_s}e_3 + A_2 + K_4 e_4\right] \\ V_{rq} = \frac{\sigma L_r}{\Phi_{sd}}\left[\frac{\mu}{J}e_1 + A_1 + K_2 e_2\right] \end{cases} \quad (28)$$

Where K_2 and K_4 are positive parameters selected to guarantee a faster dynamic of the rotor current those of the stator flux and speed.

From the above we can obtain the control laws as:

$$\dot{V}_2 = -K_1 e_1^2 - K_2 e_2^2 - K_3 e_3^2 - K_4 e_4^2 \leq 0 \quad (29)$$

The studied backstepping control is illustrated by Fig.2.

3.2. Sliding Mode Control

The method consists to calculate the equivalent and discontinuous components of control variable from an adequate surface of sliding mode chosen [10, 11].

3.2.1.Description Model

The state model can then be written as [12]:

$$\dot{X} = f(X,t) + g(X,t)U_{dq} \quad (30)$$

$$\dot{X} = \begin{bmatrix} \frac{d\Phi_{sd}}{dt} \\ \frac{d\Phi_{sq}}{dt} \\ \frac{di_{rd}}{dt} \\ \frac{di_{rq}}{dt} \end{bmatrix}; U_{dq} = \begin{bmatrix} V_{sd} \\ V_{sq} \\ V_{rd} \\ V_{rq} \end{bmatrix}; g(X,t) = \begin{bmatrix} 1 & 0 & 0 & 0 \\ 0 & 1 & 0 & 0 \\ 0 & 0 & \frac{1}{\sigma L_r} & 0 \\ 0 & 0 & 0 & \frac{1}{\sigma L_r} \end{bmatrix}$$

3.2.2.*Control Design*

Sliding surfaces represent the error between the actual and references rotor currents and are expressed as follows:

$$\begin{cases} S_d = i_{rd\_ref} - i_{rd} \\ S_q = i_{rq\_ref} - i_{rq} \end{cases} \quad (31)$$

$$f(X,t) = \begin{bmatrix} -R_s a\Phi_{sd} + R_s c\left(\sigma L_r i_{rd} + \frac{M}{L_s}\frac{V_{sq}}{\omega_s}\right) + \Phi_{sq}\omega_s \\ -R_s a\Phi_{sq} + R_s c\left(\sigma L_r i_{rq} + \frac{M}{L_s}\frac{V_{sd}}{\omega_s}\right) - \Phi_{sd}\omega_s \\ \frac{1}{\sigma L_r}\left(-R_r b\left(\sigma L_r i_{rd} + \frac{M}{L_s}\frac{V_{sq}}{\omega_s}\right) + R_r c\Phi_{sd} + \omega_r\left(\sigma L_r i_{rq} + \frac{M}{L_s}\frac{V_{sd}}{\omega_s}\right)\right) \\ \frac{1}{\sigma L_r}\left(-R_r b\left(\sigma L_r i_{rq} + \frac{M}{L_s}\frac{V_{sd}}{\omega_s}\right) + R_r c\Phi_{sq} - \omega_r\left(\sigma L_r i_{rd} + \frac{M}{L_s}\frac{V_{sq}}{\omega_s}\right)\right) \end{bmatrix}$$

V_{rd} and V_{rq} will be the two components of the control vector used to constraint the system to converge to $S_{dq} = 0$. The equivalent vector control $U_{eq_{dq}}$ is computed by imposing $\dot{S}_{dq} = 0$ so the equivalent control components are given by the eq. (32).

To obtain some good performance dynamic the control vector is imposed as follows:

$$U_{dq} = U_{eq_{dq}} + K_{dq}sign(S_{dq}) \quad (32)$$

The equivalent (dq) voltage is given by:

$$U_{eq_{dq}} = \begin{bmatrix} -\left[-R_r b\left(\sigma L_r i_{rd} + \frac{M}{L_s}\frac{V_{sq}}{\omega_s}\right) + R_r c\Phi_{sd} + \omega_r\left(\sigma L_r i_{rq} + \frac{M}{L_s}\frac{V_{sd}}{\omega_s}\right)\right] \\ -\left[-R_r b\left(\sigma L_r i_{rq} + \frac{M}{L_s}\frac{V_{sd}}{\omega_s}\right) + R_r c\Phi_{sq} - \omega_r\left(\sigma L_r i_{rd} + \frac{M}{L_s}\frac{V_{sq}}{\omega_s}\right)\right] \end{bmatrix}$$

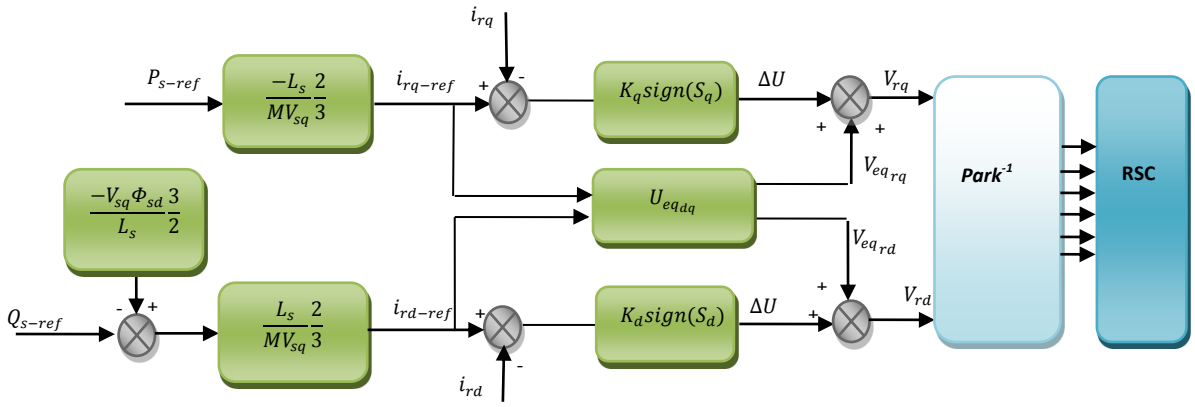

Fig. 3. Block Diagram of the proposed sliding mode applied to the RSC of WECS based on DFIG.

The nonlinear component is added to the global function of the controller in order to guarantee the attractiveness of the chosen sliding surface [19]. Considering the *Lyapunov* condition $S_{dq}\dot{S}_{dq} < 0$.

The studied sliding mode control is illustrated by Fig.3.

4. GSC Control

The grid side controller is a two-stage controller operating in a grid AC voltage reference frame. It controls the power transit with the grid via the rotor.

For the GSC, we present two control strategies. The firstly is the non linear backstepping control, the secondly is the SMC strategy.

4.1. Backstepping Control

4.1.1.Model description

The GSC is connected to the electrical grid by an intermediary line characterized by a resistance RL and a reactance XL [9]. In a reference *Park* frame related to the network angular speed **ωg** equal to the synchronous speed, the electrical voltage equation is given by:

$$\begin{cases} \frac{di_{od}}{dt} = \frac{V_{od}}{L} - \frac{R}{L}i_{od} + \omega_R i_{oq} \\ \frac{di_{oq}}{dt} = \frac{V_{oq}}{L} - \frac{R}{L}i_{oq} - \omega_R i_{od} - V_{gd} \end{cases} \quad (34)$$

The active and the reactive power are given by follows [20]:

$$\begin{cases} P_0 = \frac{3}{2}(V_{gd}i_{od} + V_{gq}i_{oq}) \\ Q_0 = \frac{3}{2}(V_{gq}i_{od} - V_{gd}i_{oq}) \end{cases} \quad (35)$$

We present in this part a study on the regulation power. This study is based on network voltage vector oriented control. This method is based on the orientation of grid voltage along Park. This implies that $V_{gd} = |\overline{V_g}|$ and $V_{gq} = 0$ [3].

In these conditions, one can write [4]:

$$\begin{cases} P_0 = \frac{3}{2}V_{gd}i_{od} \\ Q_0 = -\frac{3}{2}V_{gd}i_{oq} \end{cases} \quad (36)$$

As shown in relations (36) the dynamics of the active and reactive power are directly linked to the control of grid currents i_{od} and i_{oq}. voltage is constant and equal to the nominal AC voltage.

4.1.2.Control Design

The two tracking error e_1 and e_2 are defined by:

$$\begin{cases} e_1 = i_{od} - i_{od\_ref} \\ e_2 = i_{oq} - i_{oq\_ref} \end{cases} \quad (37)$$

The derivative of Eq. (37) gives:

$$\begin{cases} \dot{e}_1 = \dot{i}_{od} - \dot{i}_{od\_ref} \\ \dot{e}_2 = \dot{i}_{oq} - \dot{i}_{oq\_ref} \end{cases} \quad (38)$$

We must use the eq. (38) to calculate the derivative of two errors, we obtain:

$$\begin{cases} \dot{e_1} = \frac{V_{od}}{L} - \frac{\mathrm{R}}{\mathrm{L}}\mathrm{i_{od}} + \omega_\mathrm{g}\mathrm{i_{oq}} \\ \dot{e_2} = \frac{V_{oq}}{L} - \frac{\mathrm{R}}{\mathrm{L}}\mathrm{i_{oq}} - \omega_\mathrm{g}\mathrm{i_{od}} - V_{gd} \end{cases} \quad (39)$$

In order to check, let us the tracking performances choose the first *Lyapunov* candidate function V associated to the grid current errors, such us:

$$V = \frac{1}{2}(e_1^2 + e_2^2) \quad (40)$$

Using eq. (39) is written as follows:

$$\dot{\mathrm{V}} = \mathrm{e_1}\dot{\mathrm{e}}_1 + \mathrm{e_2}\dot{\mathrm{e}}_2 = \mathrm{e_1}$$
$$\frac{V_{od}}{L} - \frac{\mathrm{R}}{\mathrm{L}}\mathrm{i_{od}} + \omega_\mathrm{g}\mathrm{i_{oq}} + \mathrm{K_1}e_1) + e_2(\frac{V_{oq}}{L} - \frac{\mathrm{R}}{\mathrm{L}}\mathrm{i_{oq}} - \omega_\mathrm{g}\mathrm{i_{od}} - V_{gd} + \mathrm{K_2}e_2) - K_1e_1^2 - K_2e_2^2 \quad (41)$$

The derivative of the complete *Lyapunov* function can be negative definite, if the quantities between parentheses in eq. (41), would be chosen equal to zero.

$$\begin{cases} \frac{V_{od}}{L} - \frac{\mathrm{R}}{\mathrm{L}}\mathrm{i_{od}} + \omega_g \mathrm{i_{oq}} + \mathrm{K_1} e_1 = 0 \\ \frac{V_{oq}}{L} - \frac{\mathrm{R}}{\mathrm{L}}\mathrm{i_{oq}} - \omega_g \mathrm{i_{od}} - V_{gd} + \mathrm{K_2} e_2 = 0 \end{cases} \quad (42)$$

We deduce:

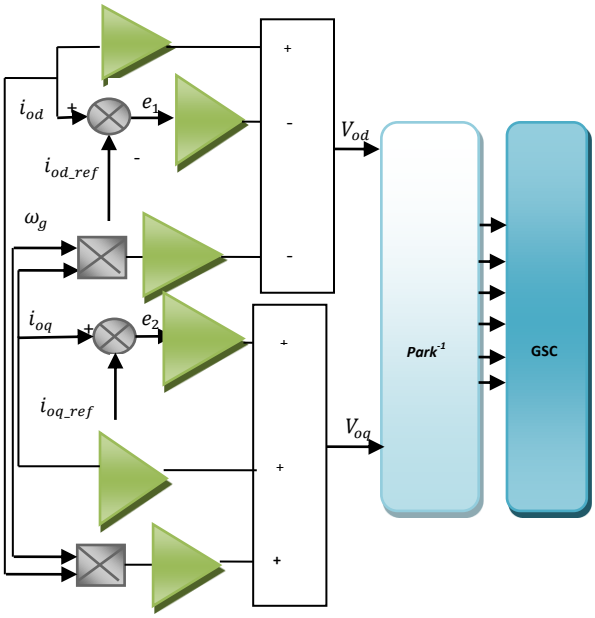

Fig. 4. Block Diagram of the proposed backstepping applied to the GSC of WECS based on DFIG.

$$\begin{cases} V_{od} = R\mathrm{i_{od}} - \omega_g \mathrm{L}\, \mathrm{i_{oq}} - \mathrm{K_1} L\, e_1 \\ V_{oq} = R\mathrm{i_{oq}} + \omega_g \mathrm{L}\, \mathrm{i_{od}} + \mathrm{L} V_{gd} - \mathrm{K_2} L\, e_2 \end{cases} \quad (43)$$

Where K_1 and K_2 are positive parameters selected to guarantee a faster dynamic of grid currents components. From the above we can obtain the control laws as:

$$\dot{V} = -K_1 e_1^2 - K_2 e_2^2 \leq 0 \quad (44)$$

The studied backstepping control is illustrated by Fig. 4.

4.2. Sliding Mode Control

4.2.1.*Control Design*

The two switching surfaces S_1 and S_2 are defined by:

$$\begin{cases} S_1 = i_{od\_ref} - i_{od} \\ S_2 = i_{oq\_ref} - i_{oq} \end{cases} \quad (45)$$

$$\begin{cases} \frac{V_{od}}{L} - \left(\frac{R_L}{L} i_{od_{ref}} - \omega_R i_{oq_{ref}}\right) = -K_1 . sign(S_1) \\ \frac{V_{oq}}{L} - \left(\frac{R_L}{L} i_{oq_{ref}} + \omega_g i_{od_{ref}} + \frac{V_{gd}}{L}\right) = -K_2 . sign(S_2) \end{cases} \quad (47)$$

In order to converge S to zero in finite time, the control law is designed such as:

$$\begin{bmatrix} \dot{S}_1 \\ \dot{S}_2 \end{bmatrix} = - \begin{bmatrix} K_1 . sign(S_1) \\ K_2 . sign(S_2) \end{bmatrix} \quad (46)$$

By the development of eq. (34) we write the eq. (47).

The GSC output currents set value are deduced as:

$$\begin{cases} i_{od\_ref} = \frac{2\, P_{o\_ref}}{3\, V_{gd}} \\ i_{oq\_ref} = -\frac{2\, Q_{o\_ref}}{3\, V_{gd}} \end{cases} \quad (48)$$

By considering eq. (47) the expression of the control voltage giving by:

$$\begin{cases} V_{od} = -K_1 L sign(S_1) + R_L i_{od_{ref}} - \omega_g L\, i_{oq_{ref}} \\ V_{oq} = -K_2 L sign(S_2) + R_L i_{oq_{ref}} + \omega_g L\, i_{od_{ref}} + V_{gd} \end{cases} \quad (49)$$

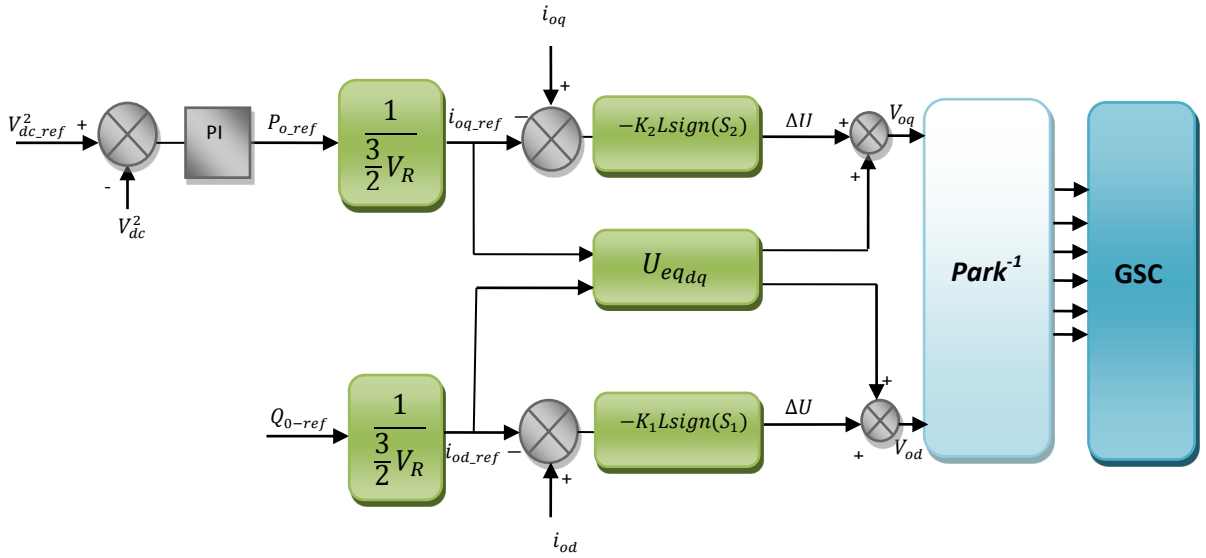

Fig. 5. Block Diagram of the proposed sliding mode applied to the GSC of WECS based on DFIG.

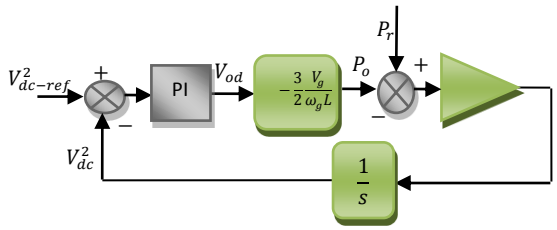

Fig. 6. Control of the DC bus voltage.

With

$$U_{eq_{dq}} = \begin{bmatrix} R_L i_{od_{ref}} - \omega_R L\, i_{oq_{ref}} \\ R_L i_{oq_{ref}} + \omega_R L\, i_{od_{ref}} + V_{gd} \end{bmatrix} \quad (50)$$

The studied sliding mode control is illustrated by Fig. 5.

4.2.2.DC Bus voltage control

The grid side ensures the DC bus voltage control as well as the exchanged active and reactive powers between the generator and the grid. Each converter exerts its influence on the DC bus by his injected current.

By neglecting the converter losses, the DC bus equation can be written as following [21]:

$$\frac{dV_{dc}^2}{dt} = \frac{2}{C}(P_r - P_o) \quad (51)$$

The filter is used to attenuate the generated harmonics by the GSC. By neglecting the filter resistor and taking into account to consider: $\Phi_{sq} = 0$, $\Phi_s = \Phi_{sd}$, $V_{sd} = 0$ and $V_{sq} = V_s$.

We obtain:

$$\begin{cases} V_{od} = -\omega_g L i_{oq} \\ V_{oq} = \omega_g L i_{od} + V_s \end{cases} \quad (52)$$

Where i_{od} and i_{oq} are the d and q components of the filter current, respectively; V_{od} and V_{oq} are the d and q components of the modulated average voltage in the filter side, respectively.

The active power transmitted into the grid through the filter is given by:

$$P_o = \frac{3}{2} V_g i_{oq} = -\frac{3}{2} V_g \frac{V_{od}}{\omega_g L} \quad (53)$$

The eq.(53) shows that the power P_o can be separately controlled by V_{od}. Consequently, it would be possible to regulate the DC bus voltage by V_{od}.

The control diagram of the DC bus voltage VC is shown in Fig. 6. The proportional integral regulator PI was introduced into the regulation loop to make null the regulation error.

5. Simulations results

Simulations results are made by using the real parameters of a wind turbine AE46 and a DFIG rated at 660KW and 690V. The operation of the WECS is simulated under the following combinations of different control strategies.

Simulations results are summarized in Table 1.

Table 1. Summarization table of simulation results illustrations.

	RSC	GSC	Figure	Location
Case1	BS	BS	8-9	Left
Case2	SMC	SMC	8-9	Right
Case3	SMC	BS	10-11	Left
Case4	BS	SMC	10-11	Right

In order to made a comparison between the proposed control strategies, all the simulations are carried out in the same operation conditions, i.e.:

- The stator flux reference is chosen equal to the nominal value 3.1Wb.
- The dc-voltage reference is equal to 1700V.
- The modeling of wind speed is a model sinusoidal is given by the following eq. (54).

In this case, we registered the response of the system to a wind presenting squalls (Fig.7) expressed in the following eq. (54).

We have summarized in Table 2, the response of the speed, torque, stator flux and rotor flux. Table 3 provides the results of comparison the performance of the devices. This summary focuses on the error of speed and torque for two different times that characterize an increase or a decrease in wind speed.

The error is defined as follows:

$$\varepsilon_X(\%) = \frac{100(X_{ref} - X)}{X_{ref}} \quad (55)$$

We remark that the combinations of proposed control strategies are able to follow the wind speed changes rapidly despite the important fluctuations of the wind speed and the big inertia of the DFIG.

$$\begin{cases} V = 3 + 10t & t < 0.7 \\ V = 10 + \sin(x) - 0.875\sin(3x) + 0.75\sin(5x) \\ -0.625\sin(10x) + 0.5\sin(30x) + 0.25\sin(50x) \\ +0.125\sin(100x) & t \geq 0.7 \end{cases} \quad (54)$$

With $x = \frac{2\pi}{10}t$

Table 2. Summarization table of the response time of different control strategies applied to WECS based on the DFIG.

RSC/GSC Response time t_r (s)	**BS/BS**	**SMC/SMC**	**SMC/BS**	**BS/SMC**
$t_{r\,\omega}$	0.5561	0.5467	0.5344	0.5984
$t_{r\,T_{em}}$	0.141	0.141	0.018	0.1472
$t_{r\,\Phi_s}$	0.213	0.191	0.178	0.244
$t_{r\,\Phi_r}$	0.287	0.251	0.14	0.301

Table 3. Summarization table for errors static of mechanical parameters of WECS based on the DFIG.

RSC/GSC	BS/BS		SMC/SMC		SMC/BS		BS/SMC	
$\varepsilon_X(\%)$	ε_ω	$\varepsilon_{T_{em}}$	ε_ω	$\varepsilon_{T_{em}}$	ε_ω	$\varepsilon_{T_{em}}$	ε_ω	$\varepsilon_{T_{em}}$
t=0.18s	1.28	41	1.28	41	1.8	12.5	1.28	41
t=2.73s	1.14	50	1.14	50	4.46	0.0633	1.14	50

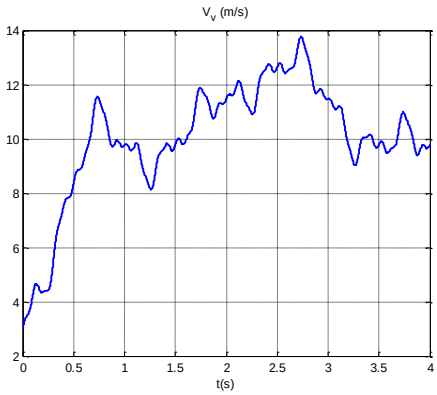

Fig. 7. Wind speed profile.

We notice that the error between the actual and reference speed is larger in the SMC/BS.

Indeed, as shown in electromagnetic torque variations illustrate by Fig. 8,10 (c,d), we observe that for a peak of wind speed, the WECS switches between the generating mode (T_{em}<0) and the motoring mode (T_{em}>0).

The stator flux is shown in Fig. 8,10 (e,f). The proposed approaches allows a quick stator flux response justified by the directly connection between the stator and the grid.

However, we notice that the BS/BS and BS/SMC strategy, the rotor flux is affected by wind variations. Indeed, as we can show in Fig.8 (g) and Fig. 10 (h), an increase, respectively, a decrease of the wind; introduce a decrease, respectively, an increase, of the rotor flux especially in the hyper synchronous mode. But the rotor flux (Fig. 8 (h), Fig. 10 (g)) is not affected by wind variations in SMC/SMC and SMC/BS.

Moreover, this wind variations have an effect on the transient's active power variations, illustrated by Fig. 9,11(c,d). This figure show that the active assessment of power is checked side stator so that: $P_s = P_{aeor} + P_r$ and $P_g = P_r + P_o$.

It is important to highlight that for all the proposed algorithms the currents in the three phase's grid, illustrate by Fig. 9,11 (e,f), constitute a balanced system of the rural grid frequency 50Hz.

According to the Table 2 and Table 3, we find that the sliding mode control SMC applied to the RSC shows high performance in terms of robustness and precision compared to backstepping control BS. While control BS applied to the GSC provides better performance than the SMC. And finally from the comparative study, we conclude that control SMC/BS offers better performance than all the control strategies developed in this paper.

6. Conclusion

This work described some control strategies applied of the wind energy conversion system WECS based on the DFIG. We have designed and compared two control strategies for the both rotor side converter (RSC) and the grid side converter (GSC): a Nonlinear backstepping control (BS) and a sliding mode control (SMC). For every proposed control, the system operates at maximum power generation mode. Simulation results of four combine control strategies BS/BS, SMC/SMC, SMC/BS and BS/SMC have proven that the proposed algorithms are able to offer convergence of the system dynamic response to the reference values despite wind variations. The SMC/BS strategy is a good candidate for controlling the WECS based on a DFIG interconnected to the grid.

References

[1] Yang L., Xu Z., Ostergaard J. and Dong ZY, "Advanced Control Strategy of DFIG Wind Turbines for Power System Fault Ride Through", IEEE Transactions on Power Systems, Vol 27, N°2, pp. 713-722, 2012.

[2] Belfedal C., Moreau S., Champenois G., Allaoui T. and Denai M, "Comparison of PI and Direct Power Control with SVM of Doubly Fed Induction Generator", Journal of Electrical & Electronics Engineering, Vol 8, N° 2, 2012.

[3] Ben Alaya J., Khedher A. and Mimouni M. F, "DTC and Nonlinear Vector Control Strategies Applied to the DFIG operated at Variable Speed", WSEAS Transactions on environment and development. Vol. 6, N° 11, pp. 744-753, 2010.

[4] Ben Alaya J., Khedher A. and Mimouni M. F, " DTC, DPC and Nonlinear Vector Control Strategies Applied to the DFIG operated at Variable Speed", Journal of Electrical Engineering JEE, Vol. 6, N° 11, pp. 744-753, 2011.

[5] Luna A., Lima F. K. A., Rodríguez P., Watanabe E. H. and Teodorescu R, "Comparison of Power Control Strategies for DFIG Wind Turbines", IEEE Transactions On Energy Conversion, pp. 2131-2136, 2008.

[6] Karthikeyan A., Kummara S.K, Nagamani C. and Saravana Ilango G, " Power control of grid connected Doubly Fed Induction Generator using Adaptive Back Stepping approach", in Proc 10th IEEE International Conference on Environment and Electrical Engineering EEEIC-2011, Rome, May 2011.

[7] Karim A., Sam Ri, "A New Approach for Maximum Power Extraction from Wind Turbine Driven by Doubly Fed Induction Generator Based on Sliding Mode Control", Energy Management, Vol 1, N° 2, 2012.

[8] Nemmour A.L., Mehazzem F., Khezzar A., M, Abdessemed R, " Advanced Backstepping controller for induction generator using multi-scalar machine model for wind power purposes", Journal of Renewable Energy, Vol . 35, N°10, pp. 2375-2380, 2010.

[9] Ben Alaya J., Khedher A., Mimouni M.F, "Variable Speed Vector Control Strategy of the Double Fed Induction Generator Integrated in Electrical Grid", Third International Conference on Ecological Vehicles & Renewable Energies (EVER'08), March 2008.

[10] Khemiri N., Khedher A. and Mimouni M.F, " Steady-state performances analysis of wind turbine using DFIG drive connected to grid", in CD-ROM of International Conference JTEA'10, Hammamet-Tunisia, 26-28 Mars 2010.

[11] Laoufi A., Hazzab A., Bousserhane I.K. and Rahli M."Direct Field-Oriented control using Backstepping technique for Induction Motor speed control", International Journal of Applied Engineering Research, vol. 1, n°1,pp. 37-50, 2006.

[12] Tan H. and Chang J, "Field orientation and adaptative Backstepping for induction motor control", Thirty-Fourth IAS Annual Meeting, IEEE Industry Applications Conference, vol. 4, pp: 2357-2363, 3-7 October1999.

[13] Trabelsi R., Khedher A., Mimouni M.F., M'Sahli F. and Masmoudi A. "Rotor flux estimation based on nonlinear feedback integrator for backstepping-controlled induction motor drives", Electromotion Journal 17, 2010, pp:163-172.

[14] Trabelsi R., Khedher A., Mimouni M.F and M'Sahli F., "An Adaptive Backstepping Observer for on-line rotor resistance adaptation", International Journal IJ-STA, Volume 4, n°1, July 2010, pp.1246-1267.

[15] Joshi R.R, Gupta R.A. and Wadhwani A.K, "Adaptive Backstepping controller design and implementation for a matrix-converter-based IM drive system", Journal of Theoretical and Applied Information Technology, JATIT, 2007.

[16] Khedher A., Mimouni M.F., Derbel N., Masmoudi A. A survey on modeling, estimation and on-line adaptation of induction motor parameters under R.F.O.C. Trans. on Systems, Signals and Devices, Vol.2, N° 2, pp.177–95, 2007.

[17] Bekakra Y. And Ben Attous D, "Sliding Mode Controls of Active and Reactive Power of a DFIG with MPPT for Variable Speed Wind Energy Conversion". Australian Journal of Basic and Applied Sciences, pp. 2274-2286, December 2011.

[18] Ouari K., Rekioua T. and Ouhrouche M. A, "Non Linear Predictive Controller for Wind Energy Conversion System", International Renewable Energy Congress IREC, pp. 220-226, November 2010.

[19] Naamane A. and Msirdi N.K, "Doubly Feed Induction Generator Control for an Urban Wind Turbine", International Renewable Energy Congress IREC, pp. 208-214, November 2010.

[20] Hu J., Nian H. and Zhu Z.Q, "Direct Active and Reactive Power Regulation of DFIG Using Sliding-Mode Control Approach". IEEE Transactions on Energy Conversion, Vol. 25, N° 4, December 2010.

[21] Jerbi L., Krichen L. and Ouali A, "A fuzzy logic supervisor for active and reactive power control of a variable speed wind energy conversion system associated to a flywheel storage system", Electric Power Systems Research, Vol. 79, No 6, pp. 919–925, 2009.

Appendix

Induction generator data

Rated power	660Kw
Rated stator voltage	400/690V
Nominal frequency	50 Hz
Number of pole pairs	n_p=2
Rotor resistance	$R_r = 0.0238\Omega$
Stator resistance	$R_s = 0.0146\Omega$
Stator inductance	$L_s = 0.0306H$
Rotor inductance	$L_r = 0.0303$
Mutual inductance	M=0.0299H

Wind turbine data

Rated power	660Kw
Blade Radius	R = 21.165 m
Power coefficient	C_{pmax} = 0.42
Optimal relative wind speed	λ_{opt}= 9
Mechanical speed multiplier	G=39
Moment of inertia	J=28 Kg.m^2
Damping coefficient	f= 0.01

Nomenclatures

P_{aeor} : The wind available power
T_t : Wind turbine torque (Nm),
V : Wind speed (m/s)
R : Blade radius (m)
ρ : Air density
β : Pitch angle
n_p: Number of pair poles
C_p : Power coefficient
Ω_t: Wind turbine angular speed (shaft speed) (rad/s)
Ω: Mechanical speed (rad/s)
λ : Relative wind speed
λ_{opt} : Optimal relative wind speed
G: Mechanical speed multiplier (gearbox)s)W
J: Moment of inertia
*f: D*amping coefficient
T_{em} : Electromagnetic torque (Nm)
V_s, V_r Stator and rotor voltage (V)
i_{sd}, i_{sq} Direct and quadrature component of the stator currents (A)
i_{rd}, i_{rq} Direct and quadrature component of the rotor currents (A)

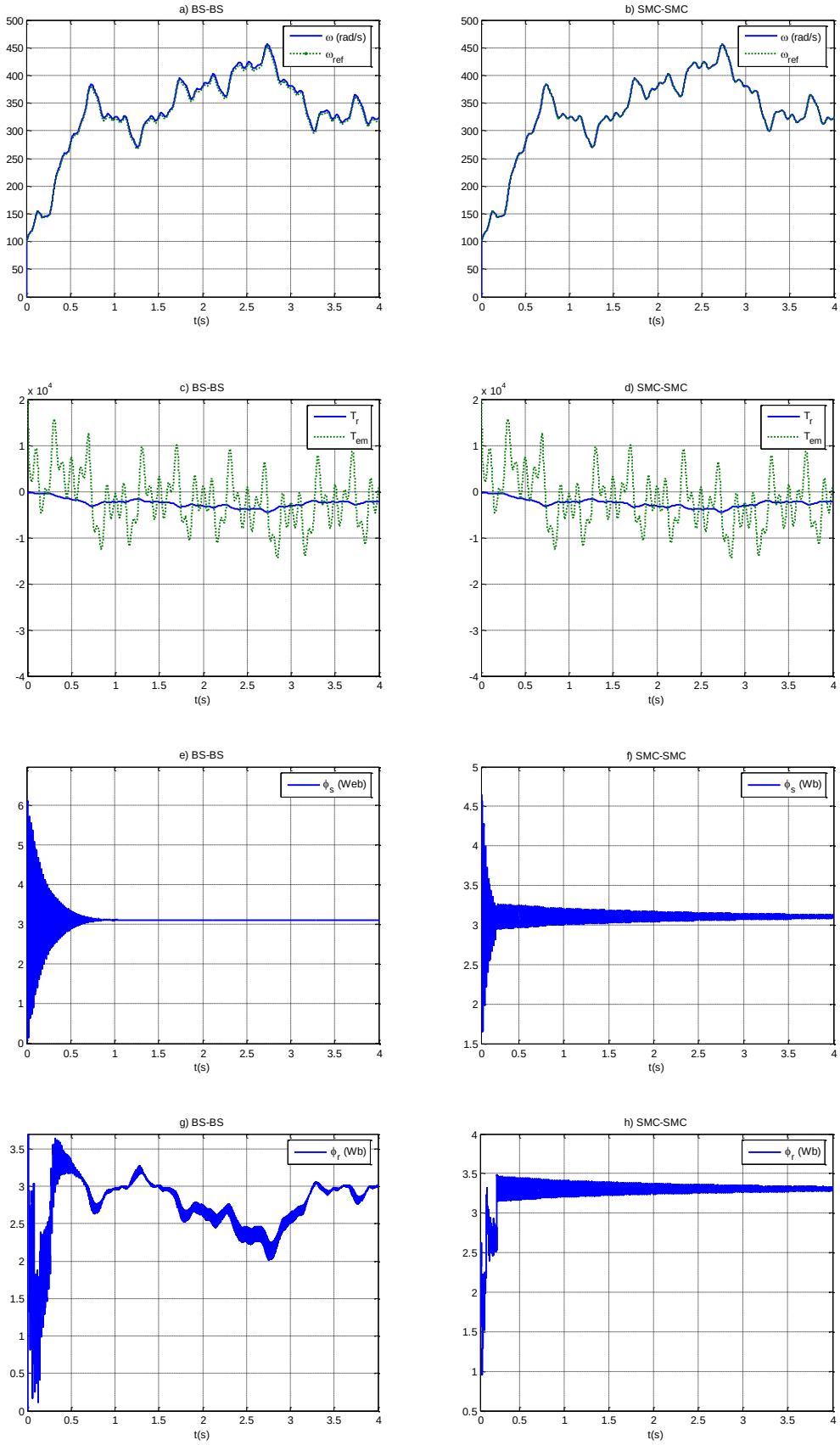

Fig. 8. WECS Response under BS-BS and SMC-SMC control strategies.
Legend: ω- ω_{ref} (a, b) , T_{em}, T_r (c, d) , φ_s (e, f), φ_r (g, h).

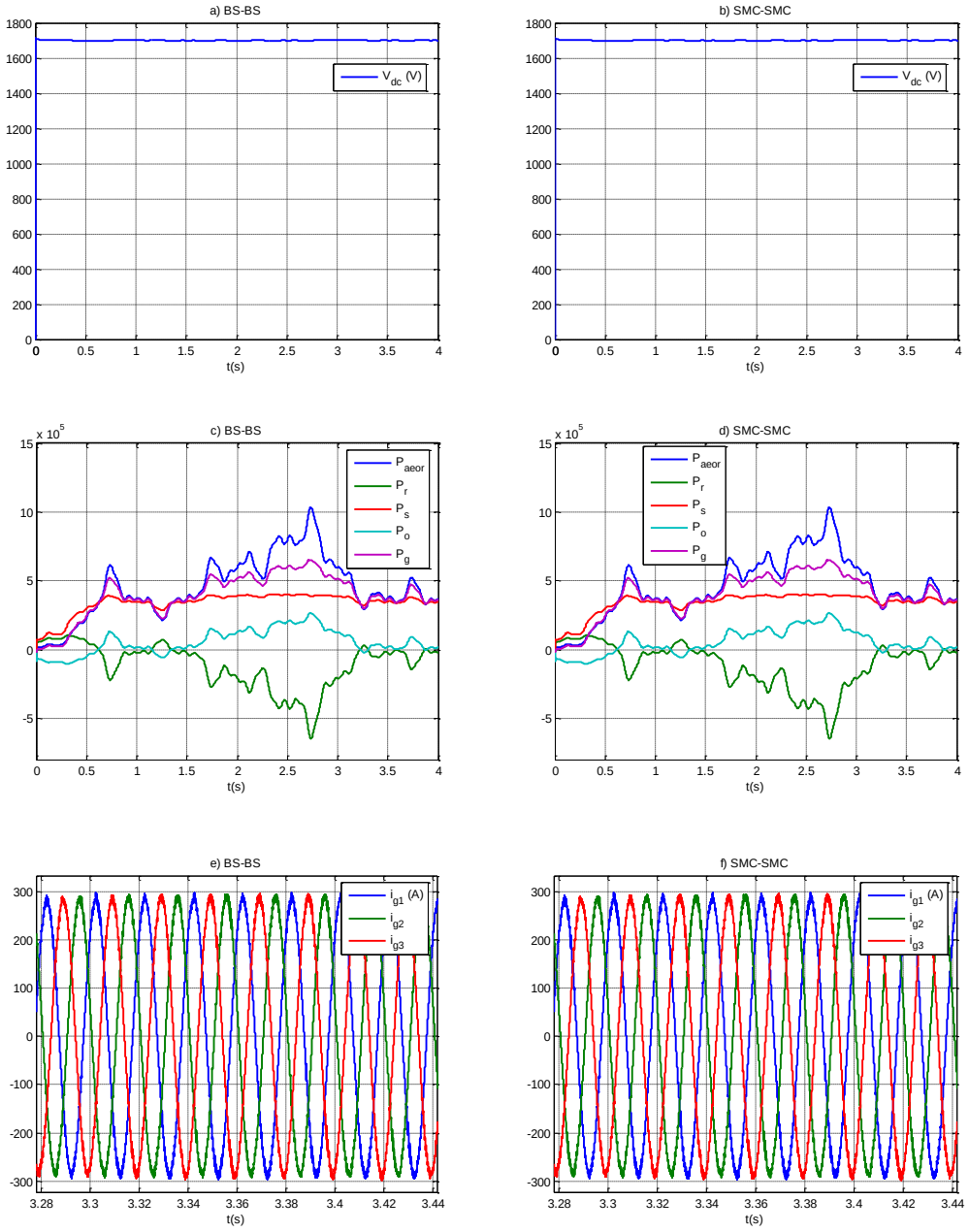

Fig. 9. WECS Response under BS/BS and SMC/SMC control strategies.
Legend: V_{dc} (a, b) , $P_{aeo,r}$ P_r , $P_{s,}$ $P_{o,}$ P_g (c,d), i_g (e,f).

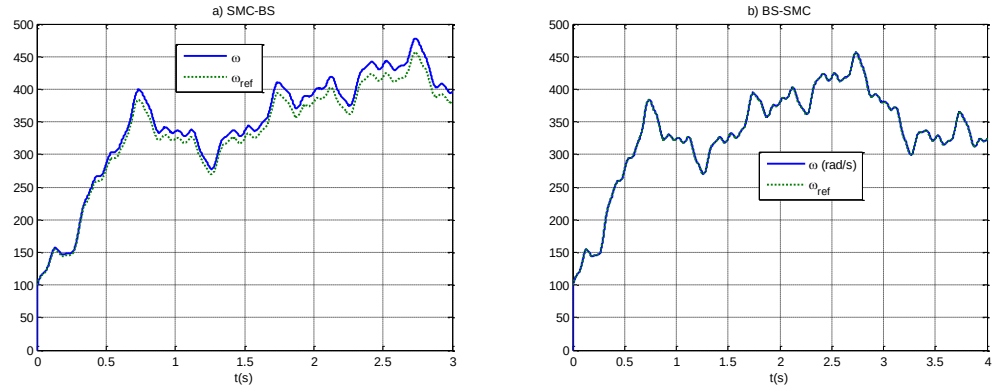

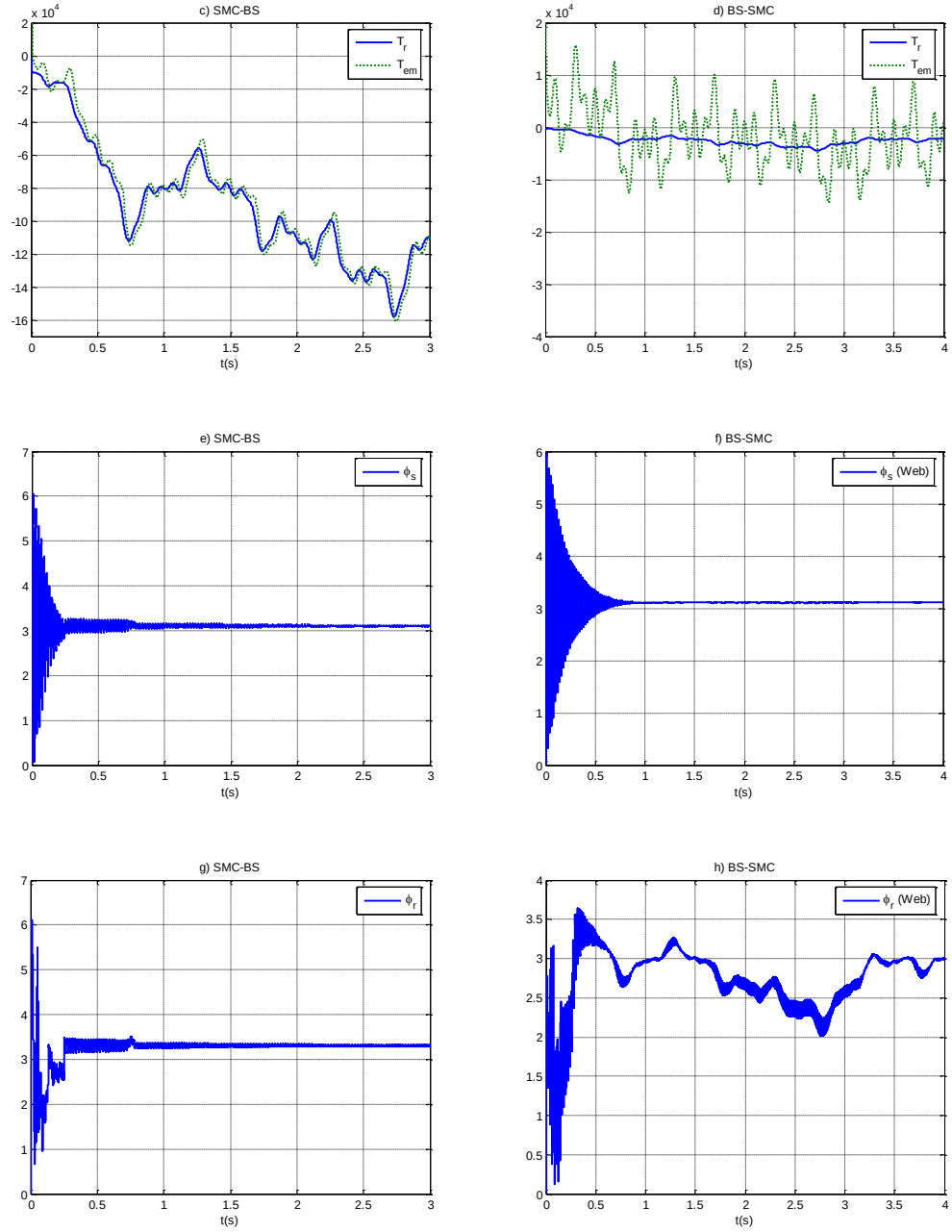

Fig. 10. WECS Response under SMC-BS and BS-SMC control strategies.
Legend: ω- ω_{ref} (a, b) , T_{em}, T_r (c, d) , ϕ_s (e, f), ϕ_r (g, h).

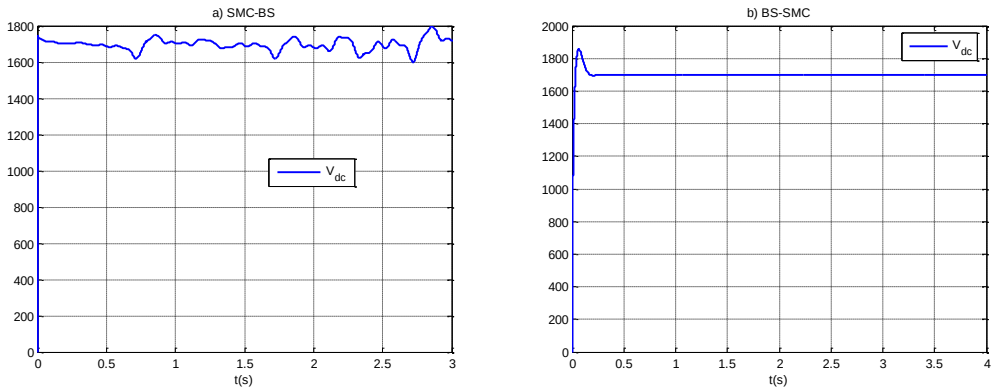

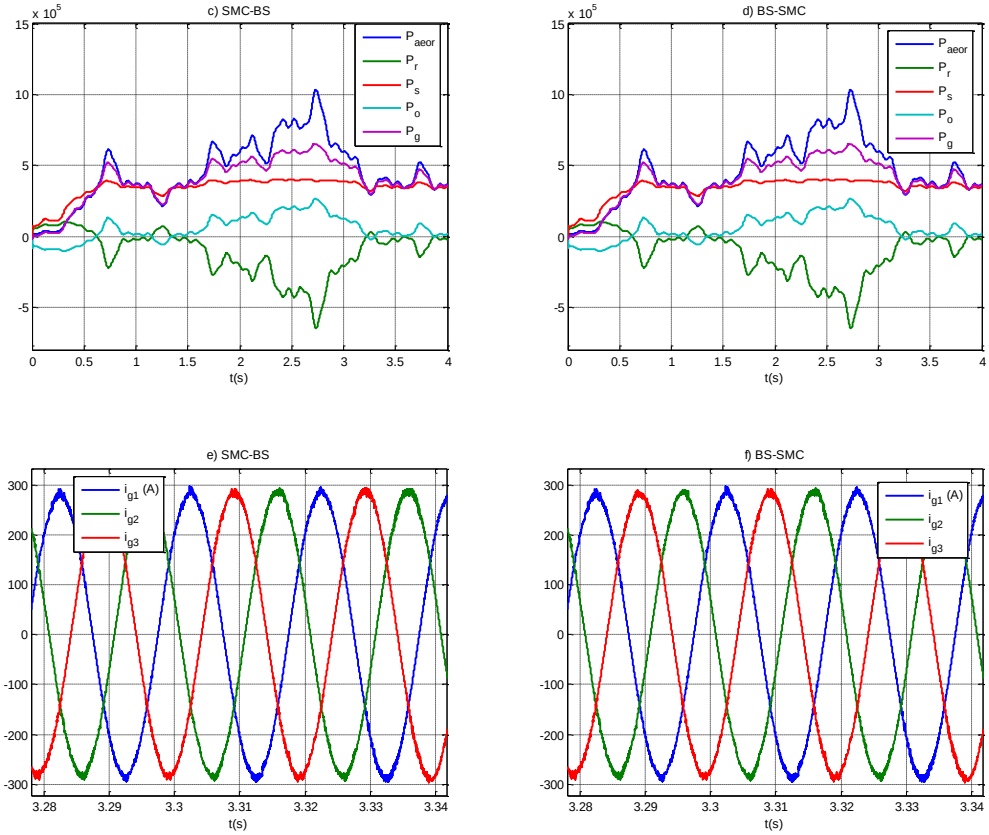

Fig.11. WECS Response under BS-BS and SMC-SMC control strategies.

Legend: V_{dc} (a, b) , $P_{aeo,r}$ P_r , $P_{s,}$ $P_{o,}$ P_g (c,d), i_g (e,f).